JACS
JOURNAL OF THE AMERICAN CHEMICAL SOCIETY
Article
pubs.acs.org/JACS

Kinetics of Isovalent (Cd^{2+}) and Aliovalent (In^{3+}) Cation Exchange in $Cd_{1-x}Mn_xSe$ Nanocrystals

Pradip Chakraborty,[†] Yu Jin,[‡] Charles J. Barrows,[†] Scott T. Dunham,[‡] and Daniel R. Gamelin*[,†]

[†]Department of Chemistry, University of Washington, Seattle, Washington 98195-1700, United States
[‡]Department of Electrical Engineering, University of Washington, Seattle, Washington 98195-2500, United States

Supporting Information

ABSTRACT: Ion exchange, in which an in-diffusing ion replaces a lattice ion, has been widely exploited as a synthetic tool for semiconductor doping and solid-to-solid chemical transformations, both in bulk and at the nanoscale. Here, we present a systematic investigation of cation-exchange reactions that involve the displacement of Mn^{2+} from CdSe nanocrystals by Cd^{2+} or In^{3+}. For both incoming cations, Mn^{2+} displacement is spontaneous but thermally activated, following Arrhenius behavior over a broad experimental temperature range. At any given temperature, cation exchange by In^{3+} is approximately 2 orders of magnitude faster than that by Cd^{2+}, illustrating a critical dependence on the incoming cation. Quantitative analysis of the kinetics data within a Fick's-law diffusion model yields diffusion barriers (E_D) and limiting diffusivities (D_0) for both incoming ions. Despite their very different kinetics, indistinguishable diffusion barriers of $E_D \approx 1.1$ eV are found for both reactions (In^{3+} and Cd^{2+}). A dramatically enhanced diffusivity is found for Mn^{2+} cation exchange by In^{3+}. Overall, these findings provide unique experimental insights into cation diffusion within colloidal semiconductor nanocrystals, contributing to our fundamental understanding of this rich and important area of nanoscience.

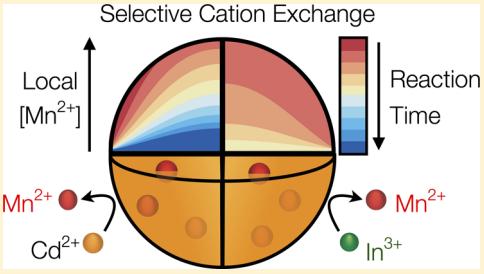

INTRODUCTION

Ion diffusion in solids is integral to many energy storage and conversion technologies, impacting, for example, solid-electrolyte kinetics in batteries and fuel cells and doping profiles in diffusion-doped semiconductor devices.[1,2] Diffusion occurs in all solids, spanning broad time and length scales, and its physical underpinnings are very generally relevant across physics, chemistry, biology, geology, and other disciplines.[3] In recent years, directed ion diffusion has become a prominent tool in the synthetic repertoire of nanoscience, enabling formation of non-equilibrium semiconductor nanostructures with exquisite compositional, shape, and size control.[4−15] Whereas broad attention has been dedicated to understanding the motions of charge carriers into and out of semiconductor nanostructures, less is known about ion mobilities in such materials. Reduced dimensionality is frequently credited with accelerating ion diffusion via increased surface-to-volume ratios, reduced transport lengths, and in some instances, altered diffusion mechanisms.[4,16−18] Although large ion mobilities may improve performance in some device technologies, it may also compromise performance in others when stable compositions are demanded at high operating temperatures. A fundamental understanding of ion diffusion in nanostructured semiconductors will thus be important for future applications of this important class of materials.

Mechanistic studies of ion diffusion in colloidal semiconductor nanocrystals are at an early stage. Experimentally, a great deal of work has been done on controlling nanocrystal compositions through cation exchange, which allows access to compositions, shapes, and heterostructures that cannot be prepared by other routes.[9,10,19,20] Cation exchange frequently involves rapidly diffusing cations such as Cu^+ or Ag^+, whose reactions are often complete within milliseconds at room temperature,[5−8] but it has also been explored with various slower-diffusing cations.[5−7,9,10,12,13] In most cases, cation diffusion is generally assumed to involve vacancy or interstitial mechanisms, with smaller ions diffusing interstitially more easily. Computational work has highlighted the importance of electrostatics in stabilizing cation vacancies during Ag^+ diffusion into CdSe nanocrystals.[21] Also computationally, energy barriers for interstitial diffusion of Mn^{2+} have been predicted to be significantly smaller in nanocrystalline CdSe ($d < 2$ nm) than in bulk CdSe, leading to greater Mn^{2+} hopping frequencies in the former.[16] Acceleration of Mn^{2+} hopping by new low-energy nanocrystal lattice vibrations was also proposed.[16] Quantitative experimental investigation of cation diffusion kinetics in semiconductor nanostructures are needed to advance the understanding, and ultimately the utility, of chemical transformations that involve ion diffusion through semiconductor nanostructures.

Here, we report a detailed investigation into the cation-exchange kinetics of a model system of free-standing colloidal semiconductor nanocrystals. Mn^{2+} ions embedded within colloidal $Cd_{1-x}Mn_xSe$ nanocrystals are expelled from these crystals by addition of Cd^{2+} and In^{3+} cations, both of which form stronger M^{n+}−Se^{2-} bonds than Mn^{2+} (Cd^{2+}−Se^{2-}, 310 kJ/mol; In^{3+}−Se^{2-}, 247 kJ/mol; Mn^{2+}−Se^{2-}, 201 kJ/mol),[22]

Received: June 9, 2016
Published: September 4, 2016

DOI: 10.1021/jacs.6b05949
J. Am. Chem. Soc. 2016, 138, 12885−12893

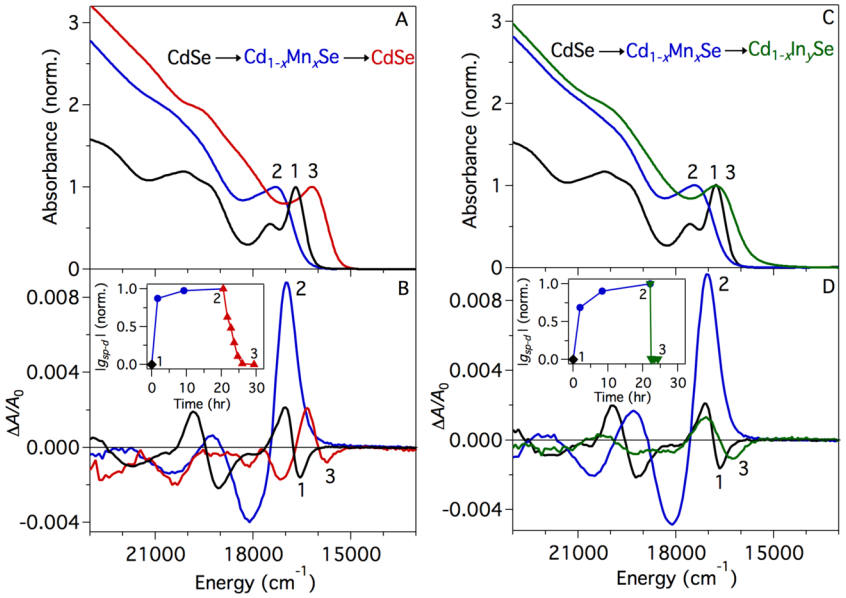

Figure 1. (A) Room-temperature electronic absorption spectra of undoped $d = 4.5 \pm 0.2$ nm CdSe nanocrystals (1, black), the same nanocrystals equilibrated after 20 h diffusion doping at 300 °C with 0.5:1:1 Se^{2-}:Mn^{2+}:CdSe (2, blue), and purified by 10 h of cation exchange with Cd^{2+} (3, red, 1:1 added Cd^{2+}:previously added Se^{2-}) at 300 °C. (B) Room-temperature MCD spectra of the same nanocrystals. Inset: Time evolution of $|g_{sp\text{-}d}|$ during diffusion doping (blue circles) and cation exchange by Cd^{2+} (red upward triangles) at 300 °C, as determined by room-temperature MCD at 1.5 T. The data are represented as the absolute value of $g_{sp\text{-}d}$ normalized to the equilibrated diffusion-doped $Cd_{1-x}Mn_xSe$ value. (C) Room-temperature electronic absorption spectra of undoped $d = 4.4 \pm 0.2$ nm CdSe nanocrystals (1, black), the same nanocrystals equilibrated after 20 h of Mn^{2+} diffusion doping at 300 °C (2, blue, 0.5:1:1 Se^{2-}:Mn^{2+}:CdSe), and after 10 min cation exchange with In^{3+} (3, green, 1:1 In^{3+}:previously added Se^{2-}) at 300 °C. (D) Room-temperature MCD spectra of the same nanocrystals. Inset: Time evolution of $|g_{sp\text{-}d}|$ during diffusion doping (blue circles) and cation exchange by In^{3+} (green downward triangles) at 300 °C, as determined by room-temperature MCD at 1.5 T.

providing a thermodynamic driving force for cation exchange. The rates of Mn^{2+} displacement by these two cations differ by nearly 2 orders of magnitude under otherwise identical conditions, with In^{3+} causing much faster Mn^{2+} expulsion from the nanocrystals. Experimental cation-exchange reaction kinetics have been measured as a function of temperature over broad temperature ranges. Fick's-law modeling of these data allows quantitative assessment of the diffusion constants and barriers for these cation-exchange reactions. The results of this analysis reveal indistinguishable diffusion barriers (E_D) for the reactions involving Cd^{2+} and In^{3+}. The vastly accelerated cation exchange when using In^{3+} could be attributed to lower effective cation activity in solution for In^{3+} (relative to Cd^{2+}) increasing the vacancy concentration in nanocrystals, or to electrostatic stabilization of lattice cation vacancies or interstitials by this aliovalent cation, emphasizing the critical role such point defects play in these chemical transformations. These results offer a unique experimental mechanistic view into cation diffusion within colloidal semiconductor nanocrystals.

EXPERIMENTAL SECTION

Nanocrystal Synthesis and Diffusion Doping. Synthesis of oleate-capped wurtzite-CdSe nanocrystals was adapted from various publications.[11,23−26] The NCs were washed by repeated suspensions in toluene and oleic acid (OA) and flocculation with ethanol. Diffusion doping of CdSe NCs with Mn^{2+} was carried out according to our previously reported procedures[11,15] for 20 h at 300 °C using 0.1 mmol (in terms of CdSe units) of CdSe seed NCs, 0.004 g (0.05 mmol) of Se powder, and 0.025 g (0.1 mmol) of $Mn(OAc)_2{\cdot}4H_2O$. Reactions were monitored by removing aliquots at various times for spectroscopic and analytical characterization.

Cation Exchange. Cation exchange was carried out from the equilibrated diffusion-doped $Cd_{1-x}Mn_xSe$ NCs between 300 and 125 °C without further purification of the reaction mixture. Solutions of cadmium oleate and indium oleate were prepared separately by adding 0.0064 g (0.05 mmol) of CdO or 0.0146 g (0.05 mmol) of indium(III) acetate, respectively, to 0.2 g of OA, and 2 g of 1-octadecene (ODE). These solutions were degassed for one hr at 115 °C to remove acetic acid and water, followed by heating to 280 °C under nitrogen until the solutions became transparent and colorless, consistent with the formation of $Cd(oleate)_2$ and $In(oleate)_3$. The solutions were then cooled to room temperature under nitrogen and added to the equilibrated diffusion-doped $Cd_{1-x}Mn_xSe$ NC solution dropwise over the course of 2 min so as not to perturb the temperature of the solution. The resulting reaction mixtures were held between 300 and 125 °C and allowed to re-equilibrate between a few minutes and several days. All the reactions were monitored by taking aliquots at various time intervals, followed by washing as described above.

Physical Characterization. Room-temperature electronic absorption spectra of all the aliquots suspended in toluene were taken in a Cary 5000 spectrometer using a 0.1 cm path length cuvette. Room-temperature magnetic circular dichroism (MCD) spectra of those aliquots were measured using the same cuvette placed in a 1.5 T electromagnet oriented in the Faraday configuration. MCD spectra were collected using an Aviv 40DS spectropolarimeter. The differential absorption of right and left circularly polarized light in the MCD experiment is reported as $\Delta A = A_L - A_R$, where A_L and A_R refer to the absorption of left and right circularly polarized photons in the sign convention of Piepho and Schatz.[27] Values of ΔE_{Zeeman}, g_{Exc}, and $g_{sp\text{-}d}$ can be calculated from these MCD data.[11,15,28−30] Based on experimental uncertainty, we estimate $\sigma \leq 5\%$ for all values of $g_{sp\text{-}d}$ reported here. TEM samples were prepared by immersing Cu grids (200 mesh, Ted Pella, Inc.) in colloidal suspensions of NCs in toluene. The grids were allowed to dry in air for a few minutes and kept inside the desiccator overnight to remove any excess water. Nanocrystal sizes from TEM and the size distribution histogram analysis were performed on ≥ 100 individual nanocrystals by using the ImageJ64 software.

DOI: 10.1021/jacs.6b05949
J. Am. Chem. Soc. 2016, 138, 12885−12893

RESULTS AND ANALYSIS

Diffusion-Doping and Cation-Exchange Reactions. Figure 1 presents electronic absorption and MCD spectra of colloidal CdSe nanocrystals measured at various stages of sequential diffusion-doping and cation-exchange reactions. Panel A shows room-temperature electronic absorption spectra of seed CdSe nanocrystals, of the same nanocrystals equilibrated after 20 h of diffusion doping with Mn^{2+},[11,15] and of the same nanocrystals after subsequent cation exchange with Cd^{2+}. The diffusion-doping and cation-exchange reactions were performed at 300 °C with the ratio 0.5:1:1 for Se^{2-}:Mn^{2+}:CdSe (where CdSe here represents lattice Cd^{2+}−Se^{2-} units) during diffusion doping, and the ratio 1:1 between added Cd^{2+} and previously added Se^{2-} during cation exchange. Diffusion doping shifts the first excitonic absorption maximum to higher energy, whereas subsequent cation exchange with Cd^{2+} shifts it to lower energy again.

Figure 1B shows corresponding room-temperature MCD spectra of the same seed CdSe nanocrystals, equilibrated diffusion-doped $Cd_{1-x}Mn_xSe$ nanocrystals, and the same nanocrystals after cation exchange with Cd^{2+}. Diffusion doping causes inversion and enhancement of the first CdSe excitonic MCD feature, whereas cation exchange inverts this feature back to a signal consistent with undoped CdSe nanocrystals. As detailed previously,[11,15] these spectroscopic changes are manifestations of Mn^{2+} diffusion into the CdSe nanocrystal lattice. Specifically, the MCD intensity inversion and enhancement seen in Figure 1B reflect the introduction of a new Mn^{2+}-exciton magnetic-exchange contribution to the excitonic Zeeman splitting upon Mn^{2+} incorporation into the CdSe nanocrystal, parametrized by the spectroscopic splitting term $g_{sp\text{-}d}$. Simultaneous analysis of the MCD and absorption spectra allows quantification of $g_{sp\text{-}d}$, which is proportional to the Mn^{2+}-exciton overlap. These spectroscopic data thus provide a quantitative measure of Mn^{2+} concentration within the CdSe nanocrystals, as verified by independent ICP-AES, TEM, and EPR measurements, allowing us to monitor the evolution of the Mn^{2+} population within the CdSe nanocrystals during diffusion doping and cation exchange.[11,15] Under these diffusion-doping conditions, x reaches ~0.15 and Mn^{2+} is distributed uniformly throughout the nanocrystal volume at equilibrium.[15] The inset of Figure 1B plots the time evolution of $|g_{sp\text{-}d}|$ (norm.) during diffusion doping and cation exchange. Here, $g_{sp\text{-}d}$ has been normalized to its maximum value achieved at equilibrium during the diffusion-doping reaction. In the undoped CdSe nanocrystals, $|g_{sp\text{-}d}| = 0$. During diffusion doping, $|g_{sp\text{-}d}|$ increases with time and eventually plateaus as the reaction approaches equilibrium. During cation exchange with Cd^{2+}, $|g_{sp\text{-}d}|$ drops and re-equilibrates at $|g_{sp\text{-}d}| = 0$ again, indicating complete removal of Mn^{2+} from the CdSe nanocrystals.

Figure 1C shows room-temperature electronic absorption spectra of undoped CdSe nanocrystals, of the same nanocrystals after 20 h of diffusion doping with Mn^{2+} at 300 °C, and of the same nanocrystals after subsequent cation exchange with In^{3+} (1:1 between added In^{3+} and previously added Se^{2-}). Diffusion doping causes a shift of the first excitonic absorption feature to higher energy, whereas cation exchange with In^{3+} shifts it back to lower energy, like cation exchange with Cd^{2+}. Figure 1D shows corresponding room-temperature MCD spectra of the same CdSe nanocrystals before and after diffusion doping, and after subsequent cation exchange with In^{3+}. MCD at the CdSe absorption edge inverts and intensifies during diffusion doping, whereas subsequent cation exchange with In^{3+} diminishes its intensity and reverts it back to the undoped CdSe-like signal. The inset of Figure 1D plots the variation of $|g_{sp\text{-}d}|$ as a function of time during diffusion doping and cation exchange. $|g_{sp\text{-}d}|$ again increases with diffusion doping time, eventually approaching a maximum, indicating Mn^{2+} in-diffusion and composition equilibration, whereas cation exchange with In^{3+} causes a rapid drop of $|g_{sp\text{-}d}|$ to zero, indicating expulsion of Mn^{2+} from the nanocrystals by In^{3+}.

Figure 2 presents TEM images and corresponding size-distribution histograms of the CdSe nanocrystals from Figure 1

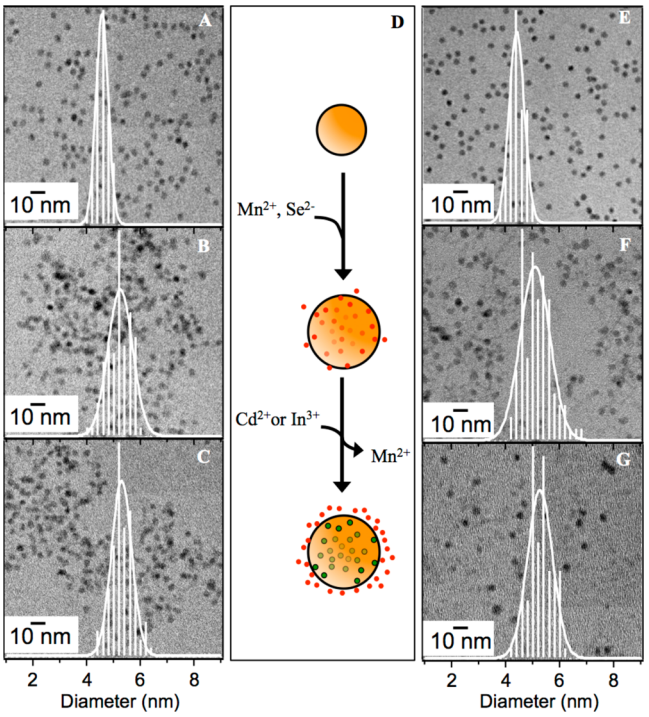

Figure 2. TEM images and size histograms (≥100 nanocrystals each) for (A) undoped CdSe nanocrystals (d = 4.5 ± 0.2 nm), (B) diffusion-doped $Cd_{1-x}Mn_xSe$ nanocrystals after 20 h diffusion doping at 300 °C (d = 5.2 ± 0.4 nm), and (C) the same nanocrystals after cation exchange with Cd^{2+} at 300 °C (d = 5.3 ± 0.3 nm). (D) Schematic illustration of CdSe nanocrystal diffusion doping by addition of Mn^{2+} and Se^{2-} to form $Cd_{1-x}Mn_xSe$ nanocrystals, followed by cation exchange with either Cd^{2+} or In^{3+} to form CdSe or $Cd_{1-x}In_ySe$ nanocrystals, respectively. TEM images and size histograms (≥100 nanocrystals each) for (E) undoped CdSe seed nanocrystals (d = 4.4 ± 0.2 nm), (F) diffusion-doped $Cd_{1-x}Mn_xSe$ nanocrystals after 20 h diffusion doping at 300 °C (d = 5.1 ± 0.5 nm), and (G) the same nanocrystals after cation exchange with In^{3+} at 300 °C (d = 5.2 ± 0.4 nm). The scale bars represent 10 nm.

during the diffusion-doping and cation-exchange reactions. Figure 2A shows the undoped CdSe nanocrystals used for the diffusion-doping and subsequent cation-exchange experiments with Cd^{2+}. These nanocrystals have an average diameter of 4.5 ± 0.2 nm (σ = 4.4%). Figure 2B shows the same nanocrystals equilibrated after 20 h of diffusion doping with Mn^{2+} at 300 °C. During diffusion doping, the average nanocrystal diameter increases to 5.2 ± 0.4 nm (σ = 7.7%) due to formal addition of Mn^{2+}−Se^{2-} units to the lattice. Figure 2C shows the same nanocrystals after subsequent cation exchange with Cd^{2+} at 300 °C. The average diameter of 5.3 ± 0.3 nm (σ = 5.6%) is essentially unchanged during cation exchange. Figure 2D illustrates

DOI: 10.1021/jacs.6b05949
J. Am. Chem. Soc. 2016, 138, 12885−12893

the CdSe nanocrystal diffusion-doping and cation-exchange reactions schematically. Figure 2E shows the undoped CdSe nanocrystals used for the diffusion-doping and subsequent cation-exchange experiments with In^{3+}. These nanocrystals have an average diameter of 4.4 ± 0.2 nm (σ = 4.5%). Figure 2F shows the same nanocrystals after 20 h of diffusion doping with Mn^{2+} at 300 °C. The average diameter increases to 5.1 ± 0.5 nm (σ = 9.8%). Figure 2G shows the same nanocrystals after subsequent cation exchange with In^{3+} at 300 °C. The average diameter of 5.2 ± 0.4 nm (σ = 7.7%) remains essentially unchanged during cation exchange. In^{3+} is clearly detected in the EDX spectrum of these nanocrystals measured after cation exchange with In^{3+} (see Supporting Information).

Figure 3 shows the variation of $|g_{sp\text{-}d}|$ (normalized to the equilibrated diffusion-doped $Cd_{1-x}Mn_xSe$ values) as a function

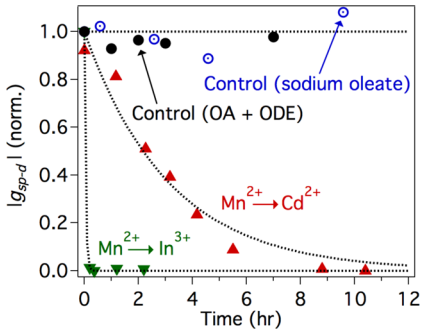

Figure 3. Time evolution of $|g_{sp\text{-}d}|$ during 300 °C cation exchange starting from equilibrated, diffusion-doped $Cd_{1-x}Mn_xSe$ nanocrystals upon addition of In^{3+} (green downward triangles, 1:1 added In^{3+} to previously added Se^{2-} during the diffusion-doping step), Cd^{2+} (red upward triangles, 1:1 added Cd^{2+} to previously added Se^{2-} during the diffusion-doping step). Data from control experiments using sodium oleate (blue circles, 1:1 added sodium oleate to previously added Se^{2-} during the diffusion-doping step) and a mixture of OA and ODE (black circles) are also included. Both control experiments were performed with 0.2 g of OA and 2 g of ODE. The dashed curves show single-exponential fits of the In^{3+} and Cd^{2+} data and horizontal lines for the sodium oleate and OA and ODE data. All experiments shown here were performed on equilibrated diffusion-doped $Cd_{1-x}Mn_xSe$ nanocrystals made by diffusion doping the same or similar undoped CdSe NCs at 300 °C for 20 h with 0.5:1:1 Se^{2-}:Mn^{2+}:CdSe mole ratios.

of time during cation exchange with Cd^{2+} or In^{3+}. Mn^{2+} removal from the $Cd_{1-x}Mn_xSe$ nanocrystal lattice during cation exchange with In^{3+} takes place in a few minutes at 300 °C, whereas it takes about 10 h during cation exchange with Cd^{2+} at the same experimental temperature. Therefore, at the same temperature, cation exchange with In^{3+} is much faster than with Cd^{2+}. Control experiments performed with sodium oleate or with only oleic acid and ODE at the same temperature result in no meaningful change in $|g_{sp\text{-}d}|$ over several hours, indicating no loss of Mn^{2+}. These control experiments exclude self-purification or ligand concentration effects under these conditions. Mn^{2+} removal from the $Cd_{1-x}Mn_xSe$ nanocrystal lattice takes place only via cation exchange with Cd^{2+} or In^{3+}. The dashed curves in Figure 3 show single-exponential fits of the Cd^{2+} and In^{3+} cation-exchange data and are included as guides to the eye (*vide infra*).

Figure 4 presents data from variable-temperature cation-exchange measurements for diffusion-doped $Cd_{1-x}Mn_xSe$ nanocrystals using Cd^{2+} or In^{3+} as the incoming cation, and plots the evolution of $|g_{sp\text{-}d}|$ as a function of temperature.

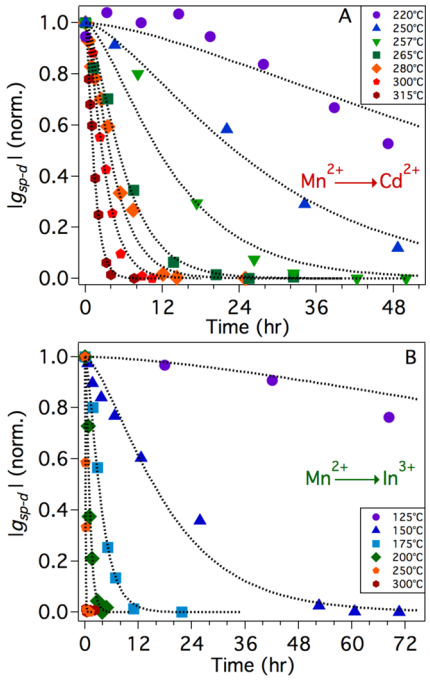

Figure 4. Temperature dependence of the cation-exchange reaction kinetics for the exchange of Mn^{2+} in d = 5.2 nm $Cd_{1-x}Mn_xSe$ nanocrystals by Cd^{2+} or In^{3+} ions. The data plot the change in $|g_{sp\text{-}d}|$ vs time for parallel reactions run at different temperatures. All measurements were performed starting with equilibrated, diffusion-doped $Cd_{1-x}Mn_xSe$ nanocrystals (20 h diffusion doping at 300 °C with 0.5:1:1 Se^{2-}:Mn^{2+}:CdSe). (A) Cation exchange with Cd^{2+}, where the ratio of added Cd^{2+} to Se^{2-} added during diffusion doping is 1:1. (B) Cation exchange with In^{3+}, where the ratio of added In^{3+} to Se^{2-} added during diffusion doping is 1:1. The dashed curves show the results of data simulation using a Fick's-law model (see text for details), from which diffusivities and diffusion barriers are quantified. Data for longer reaction times are included as Supporting Information.

The corresponding electronic absorption and MCD spectra are provided as Supporting Information. For both incoming cations, $|g_{sp\text{-}d}|$ decreases roughly exponentially with time at all temperatures, asymptotically approaching zero. Figure 4A shows that Mn^{2+} removal from the nanocrystals occurs on a time scale of several hours after the addition of Cd^{2+} across a broad range of temperatures (220–315 °C), and that the reaction gets much slower at lower temperatures. Even after one full day of Cd^{2+} cation exchange at 250 °C, $|g_{sp\text{-}d}|$ has decreased by only ~50%. By contrast, cation exchange with In^{3+} proceeds much faster (Figure 4B). Mn^{2+} displacement is complete essentially immediately upon addition of In^{3+} at 300 °C, and is complete within a few minutes of In^{3+} addition at 250 °C. Again, the reaction becomes slower with decreasing reaction temperature, but at every temperature it is still much faster than cation exchange with Cd^{2+} at the same temperature. Overall, under otherwise identical conditions, cation exchange from equilibrated $Cd_{1-x}Mn_xSe$ nanocrystals is approximately 2 orders of magnitude faster with In^{3+} than with Cd^{2+}. The dashed curves in Figure 4 show results from modeling, as described in the following section.

Modeling Mn^{2+} Diffusion Kinetics. Generally, ion diffusion through a crystal lattice involves interactions with point defects such as interstitials or vacancies. For example, in bulk II–VI and III–V semiconductors, Mn^{2+} diffusion is believed to primarily involve substitutional hopping mediated by cation vacancies.[31] Whether the out-diffusion of Mn^{2+} ions from $Cd_{1-x}Mn_xSe$

DOI: 10.1021/jacs.6b05949
J. Am. Chem. Soc. 2016, 138, 12885–12893

nanocrystals is mediated by interstitials or vacancies is *a priori* unknown. By simulating the experimental results, we aim to help identify the dominant mechanism. As will be shown, we find that mobile complexes mediating Mn^{2+} out-diffusion possess a shorter mean-free path than the nanocrystal dimensions. Since interstitials are likely to have a larger mean-free path than our very small nanocrystal dimensions, as in other material systems,[32] this conclusion suggests that Mn^{2+} out-diffusion is most likely mediated by cation vacancies. We thus propose that the mechanism for Mn^{2+} out-diffusion in our $Cd_{1-x}Mn_xSe$ nanocrystals is analogous to the vacancy-mediated mechanism of Mn^{2+} diffusion in related bulk semiconductors.[31]

In vacancy-mediated diffusion, Mn^{2+} exchanges with vacancies at neighboring lattice sites. The diffusion process can be expressed as

$$Mn^{2+} + V \leftrightarrow V + Mn^{2+} \tag{1}$$

The effective diffusivity of Mn^{2+} mediated by vacancies (D) is

$$D = nX_V^{Mn^{2+}}\Gamma_{Mn^{2+}/V}a^2/6 \tag{2}$$

Here, $X_V^{Mn^{2+}}$ is the fractional concentration of cation vacancies adjacent to Mn^{2+} ions, n is the number of adjacent sites, $\Gamma_{Mn^{2+}/V}$ represents the Mn^{2+}–vacancy exchange rate, and a is the hopping distance. In principle, D could be a function of time and position within the nanocrystal, which is difficult to characterize given the limited experimental data set. Because the chemical potential does not change much in the solution during the cation-exchange reactions reported here, we assume that the concentration of vacancies in these nanocrystals is relatively constant throughout the experiment. Also, because of the small dimensions of the nanocrystals, we assume uniform distributions of vacancies within the nanocrystals. We thus simplify the model by assuming that a single average D is applicable in any specific reaction performed under fixed conditions.

To describe the experimental ion-diffusion data quantitatively, we solve the Fick's-law diffusion equation. In a spherical coordinate system, the diffusion equation has the following form:

$$\frac{\partial u}{\partial t} = D\frac{1}{r^2}\frac{\partial}{\partial r}r^2\frac{\partial u}{\partial r}, \quad 0 < r < R \tag{3}$$

Here, the distribution function u describes the Mn^{2+} ion distribution within the nanocrystal, and D is the diffusion coefficient (diffusivity). We define the initial condition as

$$u(r, t = 0) = U_0 \tag{4}$$

where $U_0 = 1$.

To solve eq 3, two boundary conditions must be defined. At the geometric origin of the nanocrystal ($r = 0$), we have

$$\left.\frac{\partial u}{\partial r}\right|_{r=0} = 0 \tag{5}$$

A second boundary condition describing the nanocrystal/liquid interface ($r = R$) is also needed. Initial calculations were performed under the assumption of a fixed boundary condition. Specifically, we assume that Mn^{2+} solvation (i.e., displacement by solvated Cd^{2+} or In^{3+}) at the nanocrystal/liquid interface equilibrates rapidly relative to other processes such that u at R is effectively constant for the duration of the experiment:

$$u(R, t) = u_R \tag{6}$$

In our calculations, we set $u_R = 0$, meaning that Mn^{2+} ions are rapidly removed from the nanocrystals once they reach this interface. This condition is consistent with our experimental observations that MnSe shells cannot be grown on the CdSe nanocrystals under these conditions, and that MnSe also cannot be independently nucleated under these conditions.[15] Under these fixed boundary conditions, the analytical solution to eq 3 is then

$$u(r, t) = \frac{2R[U_0 - u_R]}{\pi}\sum_{n=1}^{\infty}\frac{(-1)^{n+1}}{n} \times e^{-\lambda_n^2 Dt}\frac{\sin(\lambda_n r)}{r} + u_R, \quad \lambda_n = \frac{n\pi}{R} \tag{7}$$

We note that the MCD spectroscopic approach used to gather the data in Figure 4 measures an *effective* Mn^{2+} content given by the overlap of the dopant profile and the nanocrystal's exciton wave function. To relate the calculated diffusion results to experiment, the exciton wave function amplitude was modeled using the particle-in-a-spherical-well solution detailed elsewhere,[33] and the values of $|g_{sp\text{-}d}|$ were then related to the dopant distribution $u(r)$ by projection of $u(r)$ onto this wave function. The microscopic details of this relationship are described elsewhere.[34]

Using this approach, diffusion coefficients governing the cation-exchange kinetics were evaluated for each experiment by fitting the experimental data shown in Figure 4. The first 50th orders of eq 7 were evaluated computationally. The comparison between simulated and experimental results is included in Figure 4 for both Cd^{2+} and In^{3+} cation exchange. The diffusion calculations reproduce experiment well at each temperature, with the goodness of fit worsening only for the lowest temperatures where the data themselves are least complete. These fits yield the diffusion coefficients summarized in Table 1. Cation exchange with In^{3+} at 300 °C proceeded too rapidly to fit.

Table 1. Diffusion Coefficients Obtained from Fick's-Law Analysis of the Data in Figure 4 Using Eq 7, Corresponding to the Dashed Curves Included in Figure 4

$Mn^{2+} \rightarrow Cd^{2+}$		$Mn^{2+} \rightarrow In^{3+}$	
temp (K)	diffusivity, D (nm^2/s)	temp (K)	diffusivity, D (nm^2/s)
493	1.7×10^{-6}	398	5.6×10^{-7}
523	4.6×10^{-6}	423	6.9×10^{-6}
530	9.4×10^{-6}	448	3.5×10^{-5}
538	2.1×10^{-5}	473	1.2×10^{-4}
553	2.9×10^{-5}	523	1.1×10^{-3}
573	4.2×10^{-5}		
588	9.0×10^{-5}		

As expected from visual inspection of the data, the diffusivities increase with increasing temperature, and are greater for cation exchange when using In^{3+} than when Cd^{2+} is used. Figure 5 plots the logarithm of the fitted diffusivities vs inverse temperature. Within experimental uncertainty, these plots are linear over the entire temperature range examined here, indicating that the diffusivities show Arrhenius behavior throughout this temperature range. The dashed lines in Figure 5 represent fits of the data to the Arrhenius equation (eq 8) and yield indistinguishable values of $E_D = 1.1$ eV for both Cd^{2+} and In^{3+}. As a simple cross-check, we note that a similar diffusion barrier of ~1.1 eV is also obtained

$$D = D_0 \exp(-E_D/kT) \tag{8}$$

DOI: 10.1021/jacs.6b05949
J. Am. Chem. Soc. 2016, 138, 12885–12893

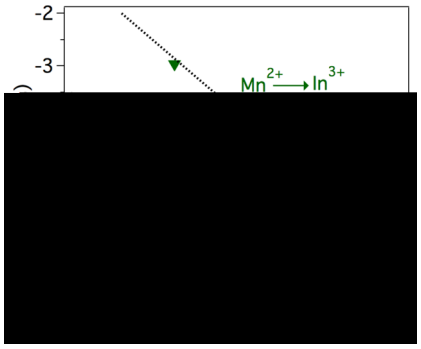

Figure 5. Arrhenius plot of the temperature dependence of the diffusion coefficients (D) measured for Mn^{2+} cation exchange by Cd^{2+} (red upward triangle) and In^{3+} (green downward triangle) in d = 5.2 nm $Cd_{1-x}Mn_xSe$ nanocrystals. The diffusion coefficients are obtained by simulating the experimental data in Figure 4 using the Fick's-law diffusion equation (eq 7) with fixed boundary conditions. The simulated curves are also depicted in Figure 4. Dashed lines show fits of the data to the Arrhenius equation (eq 8), which yield E_D = 1.1 ± 0.1 eV for both Cd^{2+} and In^{3+}. From the Arrhenius fits, limiting diffusivities of D_0 = 9.8(±1.8) × 10^4 and 2.6(±0.3) × 10^7 nm^2/s are obtained for cation exchange with Cd^{2+} and In^{3+}, respectively.

when the data in Figure 4 are fit to phenomenological single-exponential functions and the results analyzed using the Arrhenius equation (see below and Supporting Information). Despite their similar diffusion barriers, cation exchange with Cd^{2+} and In^{3+} show very different limiting diffusivities of D_0 = 9.8 × 10^4 and 2.6 × 10^7 nm^2/s for Cd^{2+} and In^{3+}, respectively. A similar increase in D_0 for Mn^{2+} diffusion is observed in $Cd_{1-x}Mn_xTe$ thin films upon co-doping with In^{3+}.[31] Because $D_0 = \nu_0 a^2$ (where ν_0 is the cation-hopping attempt frequency and a is the hopping distance), the substantial increase in D_0 when using In^{3+} relative to Cd^{2+} reflects a significant increase in Mn^{2+} hopping attempts in the former case.

For completeness, the possibility that the interface at $r = R$ cannot equilibrate fast enough to use a constant u_R was also considered. In this case, we explicitly account for the interface flux using eq 9:

$$\left.\frac{\partial u(r,t)}{\partial r}\right|_{r=R} = k \times (u(R,t) - u_{equil}(R,t)) \quad (9)$$

Here, k represents the surface equilibration rate constant, and $u_{equil}(R,t)$ describes the (quasi)equilibrium Mn^{2+} mole fraction at the nanocrystal surface. The fixed boundary condition reflects the limit of large k. If k is not sufficiently large, then surface Mn^{2+} concentrations will not be equilibrated and the diffusion profile should differ from the fixed-boundary-condition analytical solution. To verify that, we have shown the experimental and simulated curves after accounting for the interface flux at the lowest temperatures used for the Cd^{2+} and In^{3+} reactions (see Supporting Information). Very similar results are obtained using this more complete model. Although expected to be temperature dependent, effects of the interface fluxes are not detectable at lower temperatures, indicating they do not become rate limiting. This result is consistent with the finding that the diffusion coefficients extracted from the fixed-boundary-condition solution follow Arrhenius behavior at all temperatures. Overall, we conclude that surface equilibration is comparatively rapid (k is large) at all experimental temperatures explored here, and hence that the fixed boundary condition is a reasonable approximation for our present analysis.

Cation exchange via an interstitial mechanism was also considered. The interstitial process can be described as a "kick-out" mechanism. In this mechanism, interstitial Cd^{2+} (Cd_i) or In^{3+} (In_i) replaces the substitutional Mn^{2+} (Mn_s) and generates interstitial Mn^{2+} (Mn_i) as follows:

$$Cd_i + Mn_s \leftrightarrow Cd_s + Mn_i \quad (10)$$

$$In_i + Mn_s \leftrightarrow In_s + Mn_i \quad (11)$$

If the mean-free path of interstitials is much smaller than the nanocrystal dimensions (r = 2.6 nm), then we get an effective diffusivity that is indistinguishable from that of the vacancy mechanism. If, however, the mean free path of interstitials is substantially larger than the nanocrystal dimensions (e.g., the case of interstitial B in Si, where the mean free path can exceed 10 nm[32]), then Mn^{2+} out-diffusion would yield uniformly distributed Mn^{2+} throughout the nanocrystal. This uniform Mn^{2+} distribution would decay in time with a rate determined by the exchange rates of the above reactions, which can be expressed as

$$R_{Cd/Mn} = 4\pi d D_{Cd_i} C_{Cd_i} C_{Mn_s} \quad (12)$$

$$R_{In/Mn} = 4\pi d D_{In_i} C_{In_i} C_{Mn_s} \quad (13)$$

Here, d stands for effective capture distance. Using this model, we attempted to simulate the experimental data, but the goodness of fit is significantly worse than that found for the Fick's-law model. Figure 6 compares the simulations using interstitial and Fick's-law models with the experimental data for Mn^{2+} cation exchange by Cd^{2+} at 265 °C and by In^{3+} at 175 °C

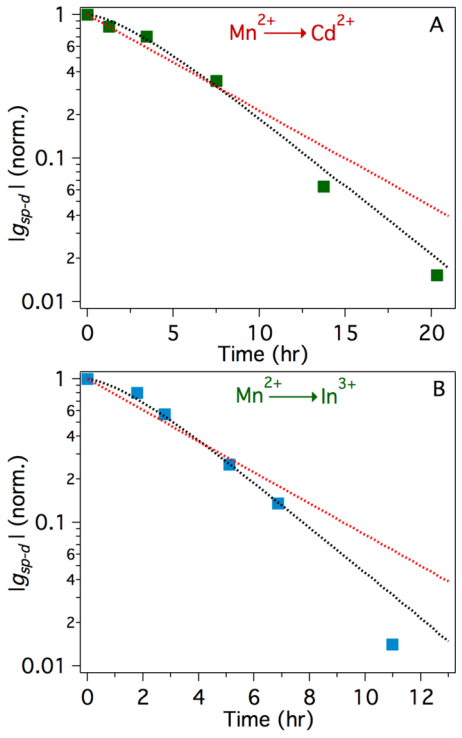

Figure 6. Comparison between experimental and simulated cation-exchange dynamics, plotted as log $|g_{sp\text{-}d}|$ vs time. (A) Mn^{2+} cation exchange by Cd^{2+} at 265 °C (experimental, green squares) and (B) Mn^{2+} cation exchange by In^{3+} at 175 °C (experimental, blue squares). Simulated curves for vacancy-mediated diffusion (black dashed) and interstitial diffusion with a large mean free path (red dashed) are included. The experimental data are from Figure 4.

DOI: 10.1021/jacs.6b05949
J. Am. Chem. Soc. 2016, 138, 12885−12893

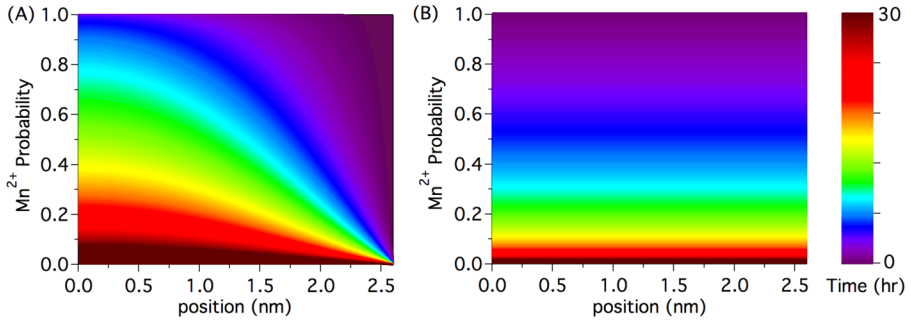

Figure 7. Contours for Mn^{2+} radial distribution evolution within d = 5.2 nm $Cd_{1-x}Mn_xSe$ nanocrystals during cation exchange with Cd^{2+} at 265 °C, calculated based on (A) vacancy-mediated diffusion with $D = 2.1 \times 10^{-5}$ nm^2/s and (B) interstitial diffusion with a mean free path of the interstitials that is larger than the nanocrystal dimension. The color bar indicates the cation-exchange reaction times of the various contours.

(selected because they have similar absolute rates). When represented on a semi-log plot, the interstitial mechanism with large mean free path yields a straight line in this plot, whereas eq 3 yields a curve. Compared to the data, the simulated data based on interstitial diffusion drop too rapidly at short times and too slowly toward the end of the reaction. The experimental data clearly deviate from linearity in a way that is consistent with Fick's law. These simulations thus favor vacancy-mediated diffusion (or an interstitial diffusion process with a short mean free path).

To highlight the difference between the vacancy-mediated and interstitial diffusion mechanisms, Figure 7 compares the evolution of the Mn^{2+} spatial distribution within a 5.2 nm CdSe nanocrystal for the two cases described by Figure 6. In the vacancy-mediated diffusion process, the Mn^{2+} concentration rapidly drops to zero at the nanocrystal/liquid interface because of rapid solvation, creating a Mn^{2+} concentration gradient within the nanocrystal. In the interstitial diffusion process, the distribution of Mn^{2+} is uniform throughout the nanocrystal and the Mn^{2+} concentration at all lattice sites decays exponentially in time during the cation-exchange reaction. This difference in Mn^{2+} spatial distribution causes discernible differences in $|g_{sp\text{-}d}|$ and gives rise to the different kinetic profiles shown in Figure 6.

DISCUSSION

The results and analysis presented here highlight the importance of the incoming cations on the kinetics of cation-exchange reactions in nanocrystals. At any given temperature, the Mn^{2+} diffusivity is ~250 times greater when using In^{3+} as the displacing cation compared to Cd^{2+} (Table 1). For both Cd^{2+} and In^{3+}, the diffusion of Mn^{2+} out of our $Cd_{1-x}Mn_xSe$ nanocrystals during cation exchange is driven thermodynamically, as summarized by the overall reactions of eqs 14 and 15.

$$[Cd_{1-x}Mn_xSe]_{NC} + xCd(oleate)_{2(sol)} \rightarrow [CdSe]_{NC} + xMn(oleate)_{2(sol)} \quad (14)$$

$$[Cd_{1-x}Mn_xSe]_{NC} + yIn(oleate)_{3(sol)} \rightarrow [Cd_{1-x}In_ySe]_{NC} + xMn(oleate)_{2(sol)} \quad (15)$$

These reactions both have equilibrium constants considerably greater than unity under our experimental conditions, despite the large excess of solvated Mn^{2+} in the reaction vessel, such that no residual lattice Mn^{2+} is detectable at equilibrium under these cation-exchange conditions. If the nanocrystal stoichiometry is determined solely by charge neutrality, then $y = (2/3)x$ in eq 15 because of the relative charges on In^{3+} and Mn^{2+}. Unfortunately, the final concentrations of In^{3+} in these nanocrystals could not be determined analytically by ICP-AES with sufficient accuracy to draw a firm conclusion about stoichiometry from this experiment, and charge compensation by excess anionic surface ligands cannot be ruled out. Interestingly, however, we find that only ~0.7 equiv of In^{3+} (per lattice Mn^{2+}) are required to displace all Mn^{2+} from the $Cd_{1-x}Mn_xSe$ nanocrystals (see Supporting Information), which is significantly less than the ~1.0 equiv of Cd^{2+} needed to achieve the same level of Mn^{2+} displacement.[15] This result is consistent with a final In^{3+} stoichiometry of $y \approx (2/3)x$.

The spontaneity of these two reactions can be qualitatively rationalized by comparing the bond strengths of their reactants and products. The greater bond enthalpies[22] of the reaction products relative to those of the reactants [Cd^{2+}–Se^{2-} (~310 kJ/mol), In^{3+}–Se^{2-} (~247 kJ/mol), Mn^{2+}–O_{oleate} (~402 kJ/mol) vs Cd^{2+}–O_{oleate} (~142 kJ/mol), In^{3+}–O_{oleate} (~360 kJ/mol), Mn^{2+}–Se^{2-} (~201 kJ/mol), gas phase, 298 K] favors spontaneous displacement of lattice Mn^{2+} by both Cd^{2+} and In^{3+} under these conditions. Other factors such as ligand concentration and the solvated ion concentrations are undoubtedly also important in determining the actual equilibrium constants of these reactions, but the critical role played by the incoming cations is confirmed by the control experiments shown in Figure 3 using sodium oleate or oleic acid in ODE alone, without addition of In^{3+} or Cd^{2+}. The lack of any detectable Mn^{2+} diffusion in these control experiments demonstrates that neither $Mn(oleate)_2$ formation nor the excess enthalpy of mixing (which prompts "self-purification") is sufficient to drive Mn^{2+} from the $Cd_{1-x}Mn_xSe$ nanocrystals under our reaction conditions. The formation of new Cd^{2+}–Se^{2-} and In^{3+}–Se^{2-} bonds is thus essential for spontaneous Mn^{2+} expulsion from these nanocrystals. This result illustrates that the incoming and outgoing cation fluxes are coupled.

The strong temperature dependence of the cation-exchange kinetics for both In^{3+} and Cd^{2+} reactions (Figures 4 and 5) reveals that the Mn^{2+} diffusion is thermally activated. Cation exchange with In^{3+} is much faster than with Cd^{2+} at any given temperature, but the data indicate the same diffusion barrier (1.1 eV) for both processes. This value of E_D is similar to those observed in analogous diffusion processes in bulk II–VI semiconductors (Table 2 and Supporting Information).

In bulk II–VI and III–V semiconductors, Mn^{2+} diffusion is believed to primarily involve substitutional hopping mediated by cation vacancies.[31] For example, cation-vacancy-mediated diffusion of single Mn^{2+} ions inside bulk wurtzite AlN single

DOI: 10.1021/jacs.6b05949
J. Am. Chem. Soc. 2016, 138, 12885–12893

Table 2. Diffusion Barriers (E_D) and Limiting Diffusivities (D_0) from This Work and Literature on Related Bulk II−VI Semiconductors

	E_D (eV)	D_0 (nm^2/s)
Mn^{2+} diffusion in Cd^{2+}:$Cd_{1-x}Mn_xSe$ ($x \approx 0.15$) nanocrystals[a]	1.1	9.8×10^4
Mn^{2+} diffusion in In^{3+}:$Cd_{1-x}Mn_xSe$ ($x \approx 0.15$) nanocrystals[a]	1.1	2.6×10^7
Mn^{2+} diffusion in CdTe/δ-MnTe/CdTe thin films[b]	1.35	1.7×10^8
Mn^{2+} diffusion in In^{3+}-doped CdTe/δ-MnTe/CdTe thin films[b,c]	1.35	4.2×10^{10}

[a]This work. [b]Ref 31. [c]$N_{In} \approx 1 \times 10^{18}$ cm^{-3}.

crystals was recently observed directly using Z-contrast STEM imaging.[35] Similarly, copper vacancies have been found to accelerate room-temperature cation exchange in $Cu_{2-x}Se$ nanocrystals.[36] The simulations presented above suggest that a related vacancy-mediated diffusion mechanism is likely also operative in our $Cd_{1-x}Mn_xSe$ nanocrystals. This conclusion is supported by the dramatic increase in D_0 for cation exchange by In^{3+} relative to Cd^{2+}. When a cation of higher charge is introduced to replace Mn^{2+} in these $Cd_{1-x}Mn_xSe$ nanocrystals, the requirement for charge neutrality can be satisfied by formation of additional compensating cation vacancies, i.e., the chemical potentials of cation vacancies are lowered. From eq 2, this change in vacancy concentration increases $X_V^{Mn^{2+}}$, which increases D. In bulk CdS and CdTe, for example, In^{3+} incorporates as In_{Cd}, with doubly ionized cation vacancies (V_{Cd}'') as the likely charge compensating defects,[37−40] and these vacancies are believed to accelerate In^{3+} diffusion.[41−43] Additionally, in the nanocrystal experiments, the combination of weaker In^{3+}−Se^{2-} and stronger In^{3+}−O_{oleate} bonds compared to Cd^{2+} should lower the effective cation activity of In^{3+} in solution relative to Cd^{2+} in solution, thereby also contributing to a larger time-averaged cation vacancy concentration. We note that the actual time-averaged vacancy concentration is unknown and may be extremely small (e.g., ≪1/nanocrystal) for both the Cd^{2+} and In^{3+} cation-exchange reaction conditions. Overall, we thus propose that Mn^{2+} cation exchange with In^{3+} in our $Cd_{1-x}Mn_xSe$ nanocrystals is accelerated relative to the same reaction performed with Cd^{2+} because In^{3+} increases the time-averaged concentration of cation vacancies. In this scenario, the experimental diffusion barriers reflect the combined activation energies of cation vacancy creation and Mn^{2+} exchange with vacant sites.

CONCLUSION

Mn^{2+} ions are spontaneously displaced from $Cd_{1-x}Mn_xSe$ nanocrystals via cation exchange when the thermodynamically preferred cations Cd^{2+} or In^{3+} are introduced to the nanocrystal solutions at elevated temperature. Under otherwise identical conditions, cation exchange is approximately 2 orders of magnitude faster when using In^{3+} compared to Cd^{2+}, illustrating the critical importance of the incoming cations. Kinetics measurements at various temperatures demonstrate that cation exchange is thermally activated for both Cd^{2+} and In^{3+} reactions, adhering to Arrhenius behavior over broad experimental temperature ranges. Quantitative analysis within a Fick's-law diffusion model yields the diffusion parameters E_D and D_0. Both cation-exchange reactions (Cd^{2+} and In^{3+}) are found to be governed by the same diffusion barrier, E_D = 1.1 eV. The large increase in D_0 (~250 times) when using In^{3+} is attributed to higher cation vacancy concentration, due either to lower effective cation activity in solution or to stabilization of charge-compensating cation vacancies. The accelerated diffusion observed when using In^{3+} to displace Mn^{2+} thus provides further evidence for cation vacancies as critical mechanistic features of these nanocrystal cation-exchange reactions. Overall, these findings provide unique experimental insights into cation diffusion within colloidal semiconductor nanocrystals, contributing to our fundamental understanding of this rich area of nanoscience and improving our ability to tailor the compositions of nanostructures for future advanced technological applications.

ASSOCIATED CONTENT

Supporting Information

The Supporting Information is available free of charge on the ACS Publications website at DOI: 10.1021/jacs.6b05949.

Additional EDX, electronic absorption, and MCD data; analysis of cation-exchange kinetics data; stoichiometry data; comparison of model results with interface flux vs fixed boundary condition; table of rate constants from analysis of cation-exchange kinetics; table of diffusion barriers and limiting diffusivities from this work and literature; and table of cation ionic radii (PDF)

AUTHOR INFORMATION

Corresponding Author

*gamelin@chem.washington.edu

Notes

The authors declare no competing financial interest.

ACKNOWLEDGMENTS

This research was funded by the U.S. National Science Foundation (DMR-1408617 to D.R.G.). P.C. acknowledges the Swiss National Science Foundation for Advanced Postdoc Mobility Fellowship (P300P2_161090). C.J.B. acknowledges Graduate Research Fellowship support from the University of Washington Clean Energy Institute.

REFERENCES

(1) Gösele, U. M. *Annu. Rev. Mater. Sci.* **1988**, *18*, 257.
(2) Fedorov, V. A.; Ganshin, V. A.; Korkishko, Y. N. *Phys. Status Solidi A* **1993**, *139*, 9.
(3) Heitjans, P.; Kärger, J. *Diffusion in Condensed Matter: Methods, Materials, Models*; Springer Science & Business Media: Berlin, 2005.
(4) Son, D. H.; Hughes, S. M.; Yin, Y.; Alivisatos, A. P. *Science* **2004**, *306*, 1009.
(5) De Trizio, L.; Manna, L. *Chem. Rev.* **2016**, DOI: 10.1021/acs.chemrev.5b00739.
(6) Beberwyck, B. J.; Surendranath, Y.; Alivisatos, A. P. *J. Phys. Chem. C* **2013**, *117*, 19759.
(7) Rivest, J. B.; Jain, P. K. *Chem. Soc. Rev.* **2013**, *42*, 89.
(8) Gupta, S.; Kershaw, S. V.; Rogach, A. L. *Adv. Mater.* **2013**, *25*, 6923.
(9) Casavola, M.; van Huis, M. A.; Bals, S.; Lambert, K.; Hens, Z.; Vanmaekelbergh, D. *Chem. Mater.* **2012**, *24*, 294.
(10) Groeneveld, E.; Witteman, L.; Lefferts, M.; Ke, X.; Bals, S.; Van Tendeloo, G.; de Mello Donega, C. *ACS Nano* **2013**, *7*, 7913.
(11) Vlaskin, V. A.; Barrows, C. J.; Erickson, C. S.; Gamelin, D. R. *J. Am. Chem. Soc.* **2013**, *135*, 14380.
(12) Justo, Y.; Sagar, L. K.; Flamee, S.; Zhao, Q.; Vantomme, A.; Hens, Z. *ACS Nano* **2014**, *8*, 7948.
(13) Fayette, M.; Robinson, R. D. *J. Mater. Chem. A* **2014**, *2*, 5965.
(14) Nedelcu, G.; Protesescu, L.; Yakunin, S.; Bodnarchuk, M. I.; Grotevent, M. J.; Kovalenko, M. V. *Nano Lett.* **2015**, *15*, 5635.

DOI: 10.1021/jacs.6b05949
J. Am. Chem. Soc. 2016, 138, 12885−12893

(15) Barrows, C. J.; Chakraborty, P.; Kornowske, L. M.; Gamelin, D. R. *ACS Nano* **2016**, *10*, 910.
(16) Chan, T.-L.; Zayak, A. T.; Dalpian, G. M.; Chelikowsky, J. R. *Phys. Rev. Lett.* **2009**, *102*, 025901.
(17) Malik, R.; Burch, D.; Bazant, M.; Ceder, G. *Nano Lett.* **2010**, *10*, 4123.
(18) Bothe, C.; Kornowski, A.; Tornatzky, H.; Schmidtke, C.; Lange, H.; Maultzsch, J.; Weller, H. *Angew. Chem., Int. Ed.* **2015**, *54*, 14183.
(19) Li, H.; Brescia, R.; Krahne, R.; Bertoni, G.; Alcocer, M. J. P.; D'Andrea, C.; Scotognella, F.; Tassone, F.; Zanella, M.; De Giorgi, M.; Manna, L. *ACS Nano* **2012**, *6*, 1637.
(20) van der Stam, W.; Bladt, E.; Rabouw, F. T.; Bals, S.; de Mello Donega, C. *ACS Nano* **2015**, *9*, 11430.
(21) Ott, F. D.; Spiegel, L. L.; Norris, D. J.; Erwin, S. C. *Phys. Rev. Lett.* **2014**, *113*, 156803.
(22) Luo, Y.-R. In *Comprehensive Handbook of Chemical Bond Energies*; Luo, Y.-R., Ed.; CRC Press: Boca Raton, FL, 2007.
(23) Carbone, L.; Nobile, C.; De Giorgi, M.; Sala, F. D.; Morello, G.; Pompa, P.; Hytch, M.; Snoeck, E.; Fiore, A.; Franchini, I. R.; Nadasan, M.; Silvestre, A. F.; Chiodo, L.; Kudera, S.; Cingolani, R.; Krahne, R.; Manna, L. *Nano Lett.* **2007**, *7*, 2942.
(24) Qu, L.; Peng, X. *J. Am. Chem. Soc.* **2002**, *124*, 2049.
(25) Yu, W. W.; Peng, X. *Angew. Chem., Int. Ed.* **2002**, *41*, 2368.
(26) Yu, W. W.; Qu, L.; Guo, W.; Peng, X. *Chem. Mater.* **2003**, *15*, 2854.
(27) Piepho, S. B.; Schatz, P. N. *Group Theory in Spectroscopy with Applications to Magnetic Circular Dichroism*; Wiley: New York, 1983.
(28) Beaulac, R.; Ochsenbein, S. T.; Gamelin, D. R. Colloidal Transition-Metal-Doped Quantum Dots. In *Nanocrystal Quantum Dots*, 2nd ed.; CRC Press: Boca Raton, FL, 2010; p 397.
(29) Furdyna, J. K. *J. Appl. Phys.* **1988**, *64*, R29.
(30) Barrows, C. J.; Vlaskin, V. A.; Gamelin, D. R. *J. Phys. Chem. Lett.* **2015**, *6*, 3076.
(31) Barcz, A.; Karczewski, G.; Wojtowicz, T.; Kossut, J. *J. Cryst. Growth* **1996**, *159*, 980.
(32) Cowern, N. E. B.; van de Walle, G. F. A.; Gravesteijn, D. J.; Vriezema, C. J. *Phys. Rev. Lett.* **1991**, *67*, 212.
(33) Norberg, N. S.; Parks, G. L.; Salley, G. M.; Gamelin, D. R. *J. Am. Chem. Soc.* **2006**, *128*, 13195.
(34) Beaulac, R.; Feng, Y.; May, J. W.; Badaeva, E.; Gamelin, D. R.; Li, X. *Phys. Rev. B: Condens. Matter Mater. Phys.* **2011**, *84*, 195324.
(35) Ishikawa, R.; Mishra, R.; Lupini, A. R.; Findlay, S. D.; Taniguchi, T.; Pantelides, S. T.; Pennycook, S. J. *Phys. Rev. Lett.* **2014**, *113*, 155501.
(36) Lesnyak, V.; Brescia, R.; Messina, G. C.; Manna, L. *J. Am. Chem. Soc.* **2015**, *137*, 9315.
(37) Kumar, V.; Kröger, F. A. *J. Solid State Chem.* **1971**, *3*, 387.
(38) Shaw, D. *J. Cryst. Growth* **1988**, *86*, 778.
(39) Chern, S. S.; Kröger, F. A. *Phys. Status Solidi A* **1974**, *25*, 215.
(40) Kato, H.; Takayanagi, S. *Jpn. J. Appl. Phys.* **1963**, *2*, 250.
(41) Jones, E. D.; Mykura, H. *J. Phys. Chem. Solids* **1978**, *39*, 11.
(42) Jones, E. D.; Vere, D. M. *J. Cryst. Growth* **1985**, *72*, 184.
(43) Watson, E.; Shaw, D. *J. Phys. C: Solid State Phys.* **1983**, *16*, 515.

DOI: 10.1021/jacs.6b05949
J. Am. Chem. Soc. 2016, 138, 12885−12893